Desalination 579 (2024) 117509

Contents lists available at ScienceDirect

Desalination

journal homepage: www.elsevier.com/locate/desal

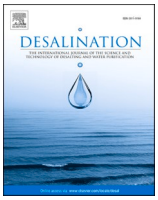

Evaluating the efficiency of modified hydrophobic PVDF membrane for the removal of PFOA substances from water by direct contact membrane distillation

Afrouz Yousefi [a], Kazem Moradi [a], Pooria Karami [a], Mostafa Dadashi Firouzjaei [b], Mark Elliott [b], Ahmad Rahimpour [a,*], Mohtada Sadrzadeh [a,*]

[a] Department of Mechanical Engineering, 10-367 Donadeo Innovation Center for Engineering, Advanced Water Research Lab (AWRL), University of Alberta, Edmonton, AB T6G 1H9, Canada
[b] Department of Civil, Construction and Environmental Engineering, University of Alabama, Tuscaloosa, AL, USA

HIGHLIGHTS

- Hydrophobic SiO_2-PVDF Membrane was fabricated for PFOA removal from wastewater.
- The membrane exhibited a water flux of 16 LMH and 95.8 % PFOA rejection.
- The membrane showed remarkable antifouling properties against PFOA substances.
- Feed inlet temperature exerts a significant impact on the membrane performance.

ARTICLE INFO

Keywords:
Per and poly-fluoroalkyl substances (PFAS)
Membrane distillation
PFOA removal
Hydrophobic membranes
Emerging contaminants

ABSTRACT

This study addresses the global issue of the contamination of water resources by *per*- and poly-fluoroalkyl substances (PFAS). PFAS are notoriously difficult to remove due to their resilient alkyl-fluorinated chains. We examined the potential of hydrophobic PVDF membranes in direct contact membrane distillation (DCMD) to eliminate perfluorooctanoic acid (PFOA) from Water. For desalination, both commercial and custom-made PVDF membranes exhibited a permeate flux of approximately 13 LMH, with salt rejections of 98.39 % and 99.95 %, respectively. In the case of PFOA removal, the fabricated PVDF membrane outperformed its commercial counterpart. It boasted an initial permeate flux of 16 LMH and a PFAS rejection of 95.8 %, compared to the commercial membrane's 13 LMH and 67.31 %. Furthermore, the custom membrane exhibited superior resistance to fouling, experiencing less flux decline. Employing response surface methodology (RSM), we identified the optimal combination of feed concentration (30 ppm), (60 °C), and flow rate (1.5 LPM) to yield a flux of 9 LMH and a PFOA rejection of 95.41 %. Feed temperature emerged as the most influential factor in DCMD performance. This study offers a novel approach to concentrating and removing emerging contaminants from wastewater and highlights the efficacy of tailored membrane technology in addressing pressing environmental challenges.

1. Introduction

Per- and poly-fluoroalkyl substances (PFASs) are a class of around 4700 fluorinated aliphatic compounds. These compounds consist of a hydrophobic, fully fluorinated alkyl chain that terminates with hydrophilic carboxylic or sulfonic acid functional groups [1]. The carbon-fluorine (C—F) bonds in the PFAS backbone structure are characterized by their robustness, requiring significant energy to break down. This strong C—F bond imparts several key properties, including chemical and thermal stability, hydrophobic and lipophilic characteristics, resistance to friction, and biotic degradation [2,3]. While these features have led to their widespread utilization in various industrial applications, such as oil and water-repellent materials found in paints, food packaging, cosmetics, lubricants, electronics, and film-forming

* Corresponding authors.
E-mail addresses: arahimpo@ualberta.ca (A. Rahimpour), sadrzade@ualberta.ca (M. Sadrzadeh).

https://doi.org/10.1016/j.desal.2024.117509
Received 25 January 2024; Received in revised form 25 February 2024; Accepted 6 March 2024
Available online 8 March 2024

foams for firefighting, they have also rendered PFAS compounds persistent in the environment due to their relatively high solubility in water [4,5].

Significant attention has been directed toward the potential hazards posed by PFAS to both human health and the environment [6]. Accumulation of PFAS compounds in the body can lead to various adverse health effects, including but not limited to cancer, obesity, elevated cholesterol levels, and impairment of kidney and thyroid function [7,8]. Given the lack of effective medical treatments for eliminating PFAS from the human body, prompt removal of these substances from the environment becomes paramount [9]. To address this concern, the United States Environmental Protection Agency (EPA) has established strict guidelines, setting total lifetime health advisory (LTHA) limits of 4 pg/L and 20 pg/L for the two most prevalent PFAS compounds, namely perfluorooctanoic acid (PFOA) and perfluorooctanesulfonic acid (PFOS), respectively, in drinking water [10]. As a result, public health regulations highlight the urgency for the water industry to develop innovative PFAS treatment methods aimed at preventing or mitigating the infiltration of these chemicals into groundwater, surface water, and ecosystems [11,12].

Over the past two decades, researchers have explored various techniques for PFAS remediation, including adsorption [13], oxidation [13,14], filtration [15], thermal [16], and biological treatments. However, these conventional methods are not sufficiently effective in eliminating PFAS from water sources due to PFAS's small molecular size, high mobility, and rapid diffusion [17–21]. Additionally, these approaches often suffer from substantial operational costs and high energy and chemical use [22]. In this context, membrane separation techniques are highly efficient methods for removing PFAS from natural water sources, offering exceptional removal efficiency, low energy consumption, ease of operation, compact design, and minimal environmental impact [23,24]. Furthermore, evaporative separation techniques can effectively concentrate PFAS from liquid solutions, primarily because PFAS compounds possess low vapor pressures and do not readily evaporate at elevated temperatures [25,26]. When heated, the water in the PFAS solution vaporizes, while the PFAS compounds remain in a liquid state [27,28]. Hence, the integration of membrane technology with evaporative techniques in an emerging membrane distillation (MD) method presents an intriguing opportunity for PFAS removal from water. MD relies on water transport through a hydrophobic membrane with relatively large pores, driven by a partial vapor pressure difference resulting from a thermal gradient [29,30]. Commonly employed membrane materials in MD, such as polyvinylidene fluoride (PVDF) and polytetrafluoroethylene (PTFE), are chosen for their hydrophobic characteristics and superior thermal stability [31,32].

One of the primary challenges affecting the prolonged use of PVDF and PTFE membranes is wetting and fouling by low surface tension substances, leading to a notable reduction in vapor flux. As an example, Chen et al. [33] employed PTFE membranes in DCMD to remove perfluoropentanoic acid (PFPeA) and observed substantial fouling of these membranes during the initial concentration hours. PFPeA from the feed gradually adhered to the surface of the PTFE membranes, and not only did the molecules remain on the surface, but they also began permeating through the membrane pores. This diffusion of PFPeA through the membrane pores resulted in a gradual decline in rejection efficiency. Therefore, modifying the membrane to mitigate wetting and address potential PFAS diffusion challenges is essential. The membrane surface characteristics, including pore dimensions, hydrophobicity, and surface charge, play a significant role in the fouling, scaling, and wetting properties of MD membranes [34]. Consequently, selecting an appropriate membrane material and implementing subsequent modifications are of great significance for the MD process. The previous research efforts have primarily concentrated on manipulating surface wettability by chemical grafting or coating advanced functional materials to the surface of MD membranes, aiming to achieve superhydrophobicity [35–40], omniphobicity [41–43], and hydrophilicity [44–47]. While MD membranes with tailored surface wettability have demonstrated success in treating specific feed water solutions, these membranes continue to face challenges due to the low stability of their coated/grafted materials. This issue hampers their prolonged operation in MD systems, ultimately impacting desalination performance and resistance to wetting. One such approach involves incorporating advanced nanoparticles, such as graphene oxide, carbon nanotubes, metal-organic frameworks (MOFs), and ZnO, into the membrane matrix to produce nanocomposite membranes and adjust the surface pore diameter and roughness, thereby improving both hydrophobicity and liquid entry pressure (LEP) [44,48–50] Zhang et al. [51] applied a hydrophilic layer composed of aluminum fumarate (AlFu) metal-organic framework (MOF) incorporated into poly (vinyl alcohol) (PVA) on a hydrophobic PTFE membrane for direct contact membrane distillation, aiming to eliminate PFAS from landfill leachate. Their results revealed that the addition of AlFu MOF enhanced PFAS and ammonia rejection by the PVA layer. Additionally, the hydrophilic layer, with or without MOF, exhibited improved resistance to wetting, and the incorporation of AlFu MOF effectively addressed the irreversible fouling.

This study uniquely employs a hydrophobic PVDF nanocomposite membrane, modified with SiO_2 nanoparticles, for the first-time application in PFAS removal through the DCMD process, with a particular focus on efficiently concentrating and removing PFOA. Furthermore, our research marks a significant advancement by introducing a semi-continuous casting machine for the scaled-up production of hydrophobic nanoparticle-polymer membranes. The main goal of the study was to improve the PVDF membrane's performance in terms of flux stability and PFOA retention. Additionally, the study aimed to optimize the operational parameters of the DCMD process to achieve enhanced PFOA removal. In this regard, a modified PVDF membrane was fabricated, and its performance was compared with commercial PVDF membranes for PFOA removal through the DCMD process. The fouling resistance and anti-wetting properties of membranes was also examined. Over the course of extensive long-term experiments, the membrane exhibited impressive anti-wetting properties, effectively preventing fouling and consistently maintaining its performance.

2. Materials and methods

2.1. Material

PVDF microfiltration membranes (0.3 μm pores) were purchased from Sterlitech *Co*. (WA, USA) and used as a commercial hydrophobic membrane in the DCMD process. PVDF powder (PVDF SOLEF® 6020/1001, Solvay Specialty Polymers) and dimethylacetamide (DMAc, >99 %, Sigma-Aldrich) were utilized to fabricate flat sheet hydrophobic PVDF membranes. Silicon dioxide (SiO_2, SkySpring Nanomaterials, Inc.) and lithium chloride (LiCl, Sigma-Aldrich) were added to the dope solution as additives to improve the hydrophobicity and pore formation, respectively. Also, PFOA (MW = 414.07 g/mol) was procured from Sigma Aldrich and dissolved in deionized water to prepare a feed solution. Deionized water with a resistivity of 18.2 M cm^{-1} (Milli-Q, Millipore) was used for both the feed solution and the coagulation bath.

2.2. Membrane preparation procedure

Fig. 1 shows the fabrication procedure for preparing hydrophobic PVDF flat sheet membrane by phase inversion via immersion precipitation technique. The dope solution was prepared first by mixing LiCl (5 wt%), SiO_2 (2 wt%), and DMAc (81 wt%). PVDF (12 wt%) was then added to the dope solution while stirring at 300 rpm and 60 °C for 24 h. The polymer solution was then degassed in a vacuum oven at room temperature for 1 h. The prepared polymer solution was carefully poured onto the polyester support mounted on a semi-continuous casting machine (Fig. S1). The casting machine facilitates uniform and controlled solution spreading, ensuring a consistent membrane

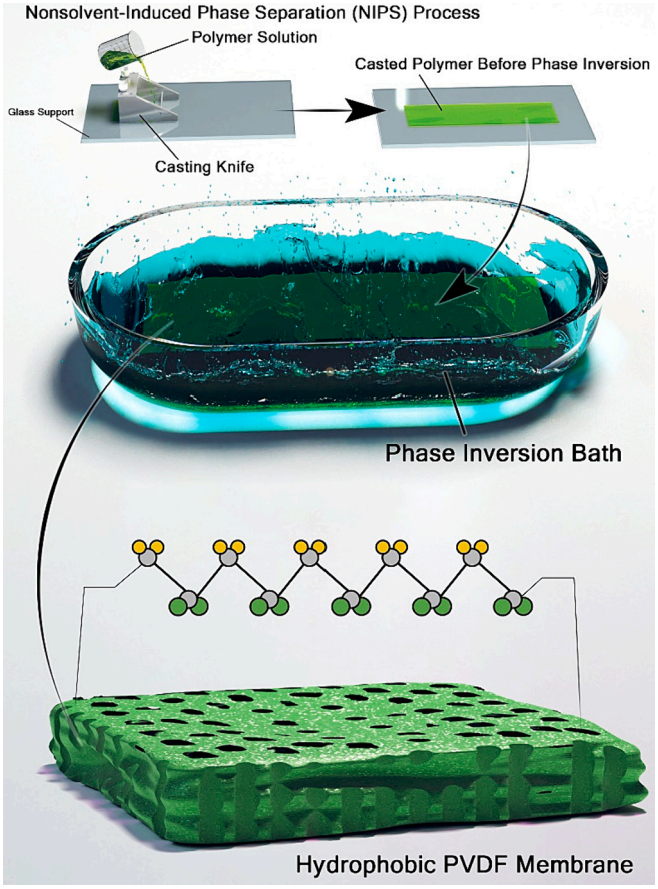

Fig. 1. Schematic representation of nonsolvent-induced phase separation (NIPS) process used in this study to fabricate hydrophobic PVDF membranes.

thickness of 0.16 μm. Subsequently, the cast film is immediately immersed in a non-solvent bath of deionized water at room temperature, where, upon completion of phase inversion and removal of residual solvents and additives, the solidified polymer sheet is rolled up. Following the collection of the polymer sheet, it undergoes a 24-h soaking in deionized water at ambient temperature, followed by sequential soaking in ethanol and n-hexane for 15 min each, aiming to minimize shrinkage effects by gradually reducing surface tension during the drying process. The final step involves drying the membrane for 24 h at room temperature.

2.3. Membrane characterization methods

Membranes' surface and cross-section morphology were examined by field emission scanning electron microscopy (FESEM, Zeiss Sigma 300 VP) at the acceleration voltage of 15 kV. The samples were first immersed in liquid nitrogen and then fractured carefully for cross-sectional FESEM imaging. Also, the elemental composition of membranes was obtained using energy dispersive spectroscopy (EDS).

The pore size of the membranes was determined through analysis of FESEM images using ImageJ software. Assuming that the pores are cylindrical, the average pore size was evaluated using the equation:

$$d_s = \left[\frac{\sum_{i=1}^{n} ni\ di^2}{\sum_{i=1}^{n} ni}\right]^{0.5} \quad (1)$$

where d_s is the average pore diameter, d_i is the ith pore diameter, n_i is the number of pores with diameter d_i, and n is the total number of pores considered.

The evaluation of membrane surface wettability was conducted through water contact angle (WCA) analysis. A 2 mL droplet of DI water in the air was used in the sessile drop measurement technique, employing a contact angle analyzer (Kruss DSA 100 Gmbh, Germany). The water droplet was placed on the membrane's surface using a micro syringe. At least three droplets were placed on the surface for each sample, and the average contact angles were subsequently determined.

The membrane surface roughness was measured by a tapping mode atomic force microscopy (AFM, Dimension ICON, Bruker, Germany). Measurements were carried out using a silicon nitride probe, scanning over a 10 μm × 10 μm area at a rate of 1 Hz. The collected data were analyzed using NanoScope Analysis software (Version 1.40r3, Bruker, Germany), and the root-mean-square roughness (R_a) was reported for each sample.

The Surpass™ 3 Electrokinetic analyzer (Anton Paar, Graz, Austria) was used to assess the zeta potential of the membranes. To measure the zeta potential values within the pH range of 4–9, a 1 mM KCl solution was utilized, and the pH was adjusted to the desired values with NaOH and HCl.

The chemical composition of the fabricated hydrophobic PVDF membranes was investigated by analyzing the surface functional groups of the membrane sample using attenuated total reflectance-Fourier transform infrared (ATR-FTIR). An Agilent Technologies Cary 600 series instrument was employed to measure infrared spectra at room temperature. The sample underwent thirty scans within the 400–4000 cm^{-1} wavelength range. For precise determination of PFAS content on a fouled membrane surface, sensitive and quantitative methods such as X-ray photoelectron spectroscopy (XPS) were considered. This technique was used to reveal the C and F bonds of PFAS on the membrane surface, as quantitatively evaluating fluoride content across a PVDF base membrane fouled with high molecular content fluoride-containing molecules like PFAS would not be practical using FTIR. The elemental composition and chemical bonding of both pristine and used membranes were evaluated using the Kratos AXIS ULTRA XPS, equipped with a monochromatic *Al* Kα X-ray source.

The liquid entry pressure (LEP) of the membranes was determined using a dead-end filtration cell. At room temperature, 200 mL of deionized water was poured into a static liquid reservoir with a membrane sample at the bottom. Pressure on the liquid was applied using compressed nitrogen from a cylinder, and the increment was controlled with a regulator at 2 psi every 10 min until water began to drop constantly from the cell outlet. Three samples were analyzed for each membrane, and the average result was reported.

2.4. Membrane transport performance evaluation

The removal of PFOA from the aqueous solution containing 10, 20, and 30 ppm of PFOA was evaluated by performing DCMD tests for the fabricated and commercial PVDF membranes. A laboratory-scale crossflow filtration MD cell (Sterlitech *Co.*) with a membrane-active area of 140 cm^2 was used. The membrane module was placed vertically, allowing the feed solution and cooling water to flow from the bottom to the top of the module. Liquid-jacketed borosilicate glass vessels with double-walled casings contained hot and cold-water solutions. To maintain the hot feed solution at a constant temperature (50, 60, and 70 °C), the Thermo Scientific heated bath (Cole-Parmer Canada *Co.*) was used to circulate the water around the vessel. A benchtop chiller (Polyscience, Illinois, USA) was also utilized to cool down the permeate solution, maintaining its temperature at 20 °C. A digital thermometer constantly monitored the temperature of hot and cold chambers. A double-head peristaltic pump (Baoding Shenzhen Precision Pump *Co.* Ltd., China) recirculated the water in the feed and permeate chambers with various flow rates (0.5, 1, 1.5 LPM). The mass change in the cold permeate side was monitored in real time using a digital balance (Mettler Toledo, ME 4002, USA) connected to a computer for data logging. All the experiments were continued to obtain a volume concentration factor (VCF=Initial feed volume/Final feed volume) of 2. To

assess the concentration of PFOA in the feed solution and distillate, samples were collected at various time intervals, and the carbon content of these samples was determined using a total organic carbon (TOC) analyzer (Shimadzu Corporation, Analytical & Measuring Instrument Division, Jiangsu, China). The TOC removal (%) is calculated using the following equation:

$$TOC\ rejection\ (\%) = \frac{(TOC_0 - TOC_t)}{TOC_0} \times 100 \quad (2)$$

Where TOC_0 is for the initial feed solution and TOC_t is for the permeate at time t.

The distillate flux (J, LMH) was calculated by the following equation:

$$J\left(\frac{L}{m^2 h}\right) = \frac{M(kg)}{\rho\left(\frac{kg}{L}\right) A(m^2)\Delta t(h)} \quad (3)$$

where M is the mass of the permeate, ρ is the density of water, A is the effective membrane area, and Δt is the measurement time.

2.5. Response surface methodology analysis

In this study, response surface methodology (RSM) was employed to explore the correlation between the responses (permeate flow and rejection) and the variables. This approach aimed to fine-tune variable conditions and predict the optimal values for the responses. The central composite design (CCD), recognized for its efficacy in sequential experimentation, was applied to attain this objective, ensuring sufficient experimental values to assess the lack of fit [52]. Three key independent variables in this study were manipulated across three levels (−1, 0, and 1): feed temperature, feed flow rate, and feed solution concentration. The independent variables and their levels, represented in both real and coded values, are detailed in Table 1. A total of 17 experiments were conducted for these three parameters, each with three replications to minimize the errors (Table S1). Analysis of variance (ANOVA) with a 95 % confidence level was used to assess the interaction between the effective parameter and the response. The modality of the polynomial model fit was evaluated by the coefficient of determination R^2 and the adjusted R^2 (R^2_{adj}) [53,54].

3. Results and discussion

3.1. Membrane characteristics

Table 2 provides an overview of the characteristics of both commercial and fabricated hydrophobic PVDF membranes. The commercial PVDF membrane displayed an overall thickness of 210 μm and a mean pore size of 0.3 μm, whereas the fabricated hydrophobic PVDF membrane had a thickness of 160 μm and a mean pore size of 0.2 μm.

In the examination of contact angles, the commercial PVDF membrane showed a water contact angle of 75°, while the fabricated hydrophobic PVDF membrane demonstrated a significantly enhanced contact angle of 102°. This improved hydrophobicity of the fabricated membrane can be attributed primarily to the inherent hydrophobic properties of the embedded silica nanoparticles [55,56], effectively mitigating any potential detrimental impact of heightened surface roughness on WCA measurements. It is widely recognized that surface roughness inherently influences wettability by increasing the contact area available for the spreading liquid [57]. Many researchers have investigated the impact of surface roughness on contact angles, aiming to determine the level of surface smoothness at which the influence of surface roughness on contact angles can be disregarded. Busscher et al. [58] and Miller et al. [59] concluded that the impact of surface roughness on contact angles becomes negligible when the average roughness and root mean square (RMS) roughness are below 100 nm and 80 nm, respectively.

Table 1
Experimental design of the selected operating conditions, representing the range of independent experimental variables used in the RSM model.

Parameter	Symbol	-1	0	+1
Feed temperature (°C)	T_f	40	50	60
Feed flow rate (L/min)	Q_f	0.5	1	1.5
Feed concentration (ppm)	C_f	10	20	30

Table 2
Key characteristic parameters of membranes.

Parameters	Commercial Membrane	Fabricated hydrophobic PVDF membrane
Thickness (μm)	210	160
Support Thickness (μm)	130	90
Mean pore size (μm)	0.3 ± 0.05	0.2 ± 0.05
Water contact angle (°)	75 ± 2	102 ± 1
Average roughness (nm)	43.00 ± 7.00	76.30 ± 8.00
Root mean square roughness (nm)	55.17 ± 8.00	95.38 ± 14.00
LEP (psi)	10	35

Therefore, considering the data presented in Table 2, the elevated WCA observed in the fabricated nanocomposite PVDF membranes can be attributed to the inherent hydrophobic properties of the incorporated silica particles. However, even if we were to entertain the idea that the membrane roughness in this study impacts the WCA, it should be interpreted in accordance with Wenzel's equation. The Wenzel equation is an approximation that becomes increasingly accurate as the size of the liquid drop becomes significantly larger compared to the scale of surface roughness. In this context, where the drop size exceeds the roughness scale by two to three orders of magnitude, as is the case here, the application of the Wenzel equation is justified. Wenzel equation states that adding surface roughness amplifies the wettability influenced by the surface chemistry. In other words, if the surface is chemically hydrophobic, introducing surface roughness would further enhance its hydrophobicity. This principle, as articulated by Wenzel, can be described as follows [60,61]:

$$cos\theta_m = rcos\theta_y \quad (4)$$

Here, $\theta_m$represents the measured contact angle, θ_y stands for Young's contact angle, and r denotes the roughness ratio. The roughness ratio is defined as the ratio between the actual solid surface area and the projected solid surface area, with $r = 1$ indicating a smooth surface and $r > 1$ indicating a rough surface. The surface roughness of the fabricated hydrophobic PVDF membrane in this study (R_a = 76.30 nm) was notably higher than that of the commercial PVDF membrane (R_a = 43.00 nm). Since the WCA of commercial PVDF membrane is <90°, it was expected to observe an increase in the WCA of the nanocomposite PVDF membrane, based on Eq. (4). However, the significant increase in the WCA highlights the remarkable influence of incorporating hydrophobic silica particles into the membrane.

A hydrophobic surface is favorable for the MD process due to less penetration of the liquid phase into the membrane pores due to the surface tension forces while allowing the passage of the vapor molecules through it [62]. The LEP plays a crucial role in maintaining the quality of the permeate in the MD process. The fabricated hydrophobic PVDF membrane exhibited higher LEP than the commercial membrane due to its smaller pore size and higher water contact angle (Table 2). These factors—smaller pore size and increased hydrophobicity—synergistically contribute to the membrane's elevated LEP, making it more effective at preventing the unwanted passage of liquid and maintaining its anti-wetting properties during the MD process.

Fig. 2(a-d) depict FESEM images illustrating the top surface and cross-section of both the commercial PVDF and fabricated hydrophobic PVDF membranes. The images reveal a uniform and porous structure

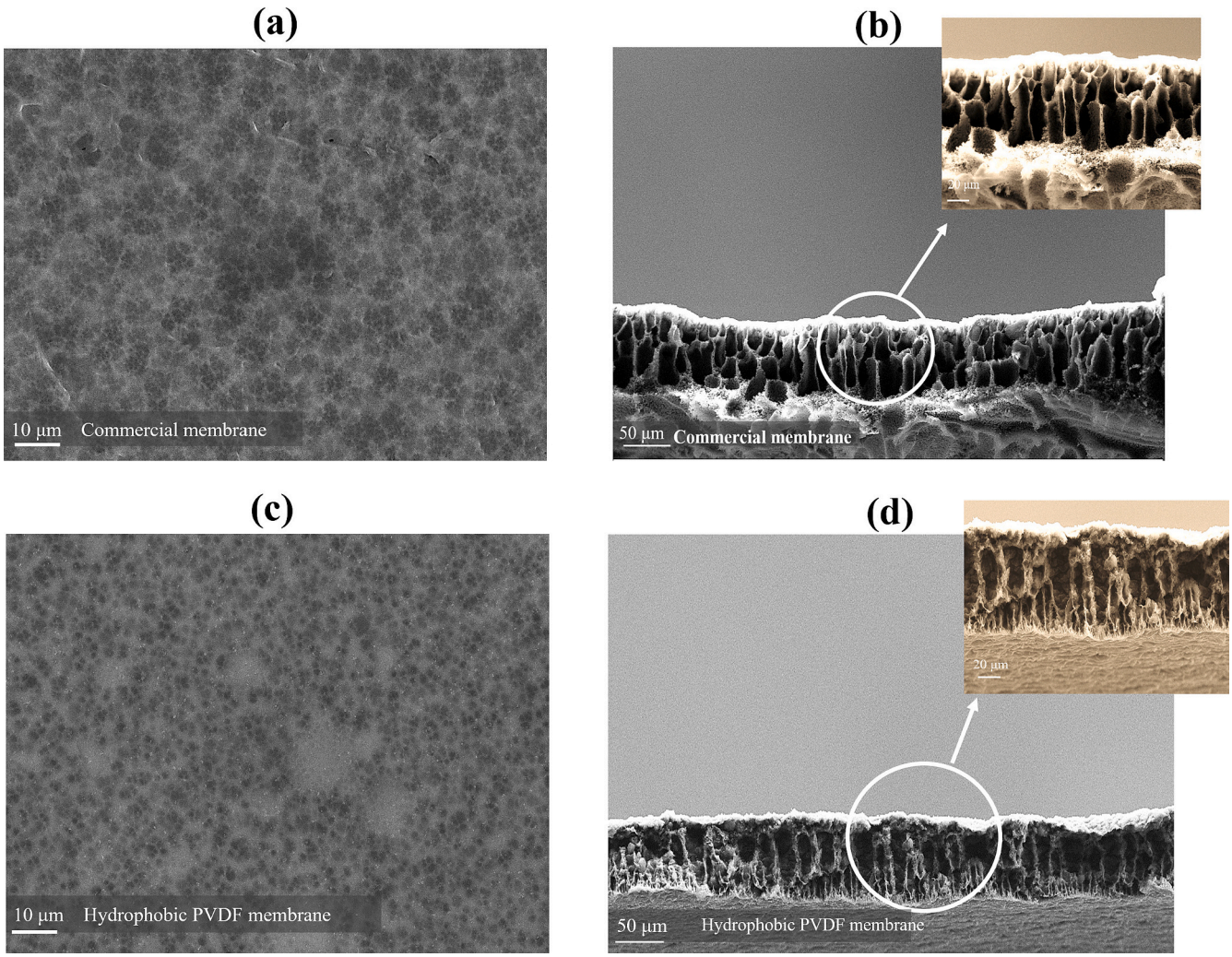

Fig. 2. (a) and (c) top FESEM images and (b) and (d) cross-sectional FESEM images of commercially fabricated hydrophobic PVDF membrane.

with a narrow pore size distribution on the top, with the fabricated membrane showing smaller pores in the top layer. Both membranes exhibit an asymmetric structure, as evidenced in Figs. 2(b) and (d), featuring a relatively thin skin layer and a finger-like substructure. Particularly, the fabricated membrane displays a more porous structure beneath the skin-selective layer. These characteristics align with the membrane feature requirements in the MD process to attain efficient performance.

Fig. 3(a) shows the FTIR spectra of the commercial and fabricated hydrophobic PVDF membranes. The characteristic peaks at 1401, 1172, and 879 cm^{-1} are attributed to the stretching and deformation vibrations of C—H_2, C—F_2, and C—C bonds in the PVDF structure, respectively. A distinctive peak at 1072 cm^{-1} is ascribed to the mixture of Si-O-C and Si-O-Si bonds of SiO_2 nanoparticles [63]. This particular peak serves as compelling evidence, unequivocally confirming the successful incorporation of SiO_2 nanoparticles into the PVDF membrane structure.

Figs. 3(b) and (c) present the EDX spectra of the commercial and fabricated hydrophobic PVDF membranes, respectively. The EDX spectrum of the fabricated hydrophobic PVDF membrane shows the presence of carbon, oxygen, fluorine, and silica elements, confirming the presence of SiO_2 nanoparticles in the structure of the PVDF nanocomposite membrane.

Fig. 3(d) presents the zeta potential results for commercial and fabricated hydrophobic PVDF membranes. Both PVDF membranes exhibited negative zeta potential values in the entire pH range, which can be attributed to the electronegative charge of C—F moieties [64]. By increasing the pH from 4 to 9, the fabricated hydrophobic PVDF membrane showed a zeta potential ranging from −27 to −36 mV, which is more negative than the commercial membrane due to the presence of SiO_2 in the membrane matrix.

The increased negativity in the zeta potential of the fabricated membrane can be attributed to the presence of SiO_2 nanoparticles within the membrane matrix. The negatively charged hydroxyl groups and silanol compounds on the surface of the SiO_2 nanoparticles contribute to this enhanced negativity [65]. SiO_2 nanoparticles typically have a low isoelectric point, indicating that they tend to carry a negative charge in aqueous solutions with a neutral pH [66]. The more negative charge of nanocomposite PVDF membranes enhances their ability to repel negatively charged PFOA molecules [67] through more pronounced electrostatic repulsion. This attribute enhances the membranes' resistance to fouling by fluorinated contaminants [68,69].

3.2. Direct Contact Membrane Distillation (DCMD) performance

3.2.1. Integrity and baseline tests

Fig. 4 depicts the flux of the membranes versus the VCF during the integrity tests with NaCl solutions. Initially, the water flux experienced a linear decline during filtration, followed by a gradual decrease attributable to the concentration polarization phenomenon. Over time, the flux stabilized as the concentration polarization layer reached a constant level [70]. The initial permeate flux for both commercial and fabricated hydrophobic PVDF membranes started at 13 LMH but eventually

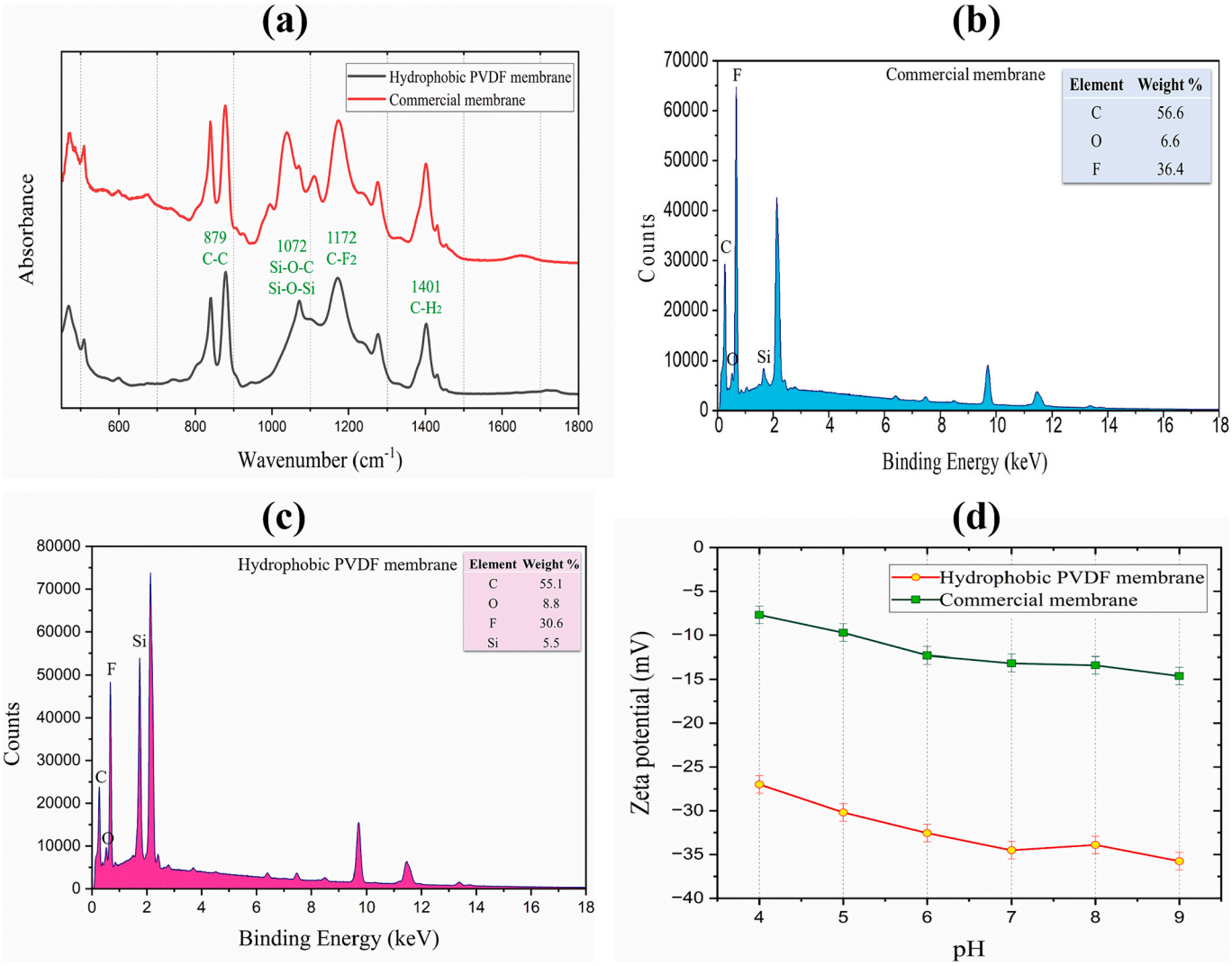

Fig. 3. (a) FTIR spectrum of the commercial and fabricated hydrophobic PVDF membrane, (b) and (c) energy-dispersive X-ray spectroscopy (EDX) spectra of commercial and fabricated hydrophobic PVDF membranes, and (d) surface zeta potential of the membranes. The zeta potential values are reported from at least three different measurements.

decreased to 11 and 10 LMH, respectively. In the MD process, water vapor molecules permeate through the membrane pores, while the diffusion of salt ions is hindered. This gradually increases salt concentration near the membrane surface on the feed side, causing concentration polarization. Concentration polarization, in turn, reduces vapor pressure on the feed side, diminishing the overall driving force. The resistance to mass transfer, influenced by the thickness of the concentration layer and the reduced driving force, consequently results in a lower mass flux [71].

Fig. 4 shows that the fabricated hydrophobic PVDF membrane consistently maintained a high salt rejection of about 99.95 % throughout the process. In contrast, the NaCl rejection of the commercial membrane decreased noticeably to 98.39 %. This reduction in salt rejection is linked to the low water contact angle of the commercial PVDF membrane (Table 2), which increases the chance of membrane wetting.

3.2.2. *PFOA removal performance of membranes*

The performance of both commercial and fabricated hydrophobic PVDF membranes in concentrating the PFOA solutions was evaluated using the DCMD process. Fig. 5 illustrates the permeate flux and rejection as a function of VCF for these membranes under identical operational conditions. The flux of fabricated nanocomposite PVDF membrane started at 16 LMH and gradually decreased to 9 LMH. In comparison, the commercial membrane exhibited an initial flux of 13 LMH, which declined to 7 LMH. The notable decline in flux during the initial filtration stage is primarily attributed to membrane fouling. Significantly, the commercial membrane experienced a substantial 50 % reduction in flux within the first eight minutes of operation, indicating more extensive fouling on its surface compared to the fabricated PVDF membrane. Under neutral pH conditions, PFOA molecules possess a negative charge attributed to the existence of a carboxyl group (-COOH) at one end of their structure [67]. Carboxylic acids have the capability to donate a proton (H^+) and transform into negatively charged carboxylate anions ($-COO^-$), with this anionic group being accountable for the negative charge of PFOA [60]:

Consequently, the fabricated hydrophobic PVDF membrane, possessing an increased negative surface charge, is more effective in repelling PFOA molecules during the MD process, leading to decreased fouling on the membrane surface [60,72]. Similarly, the fabricated membrane exhibited a more negative charge at higher pH values (Fig. 3 (d)), intensifying the electrostatic repulsion between PFOA and the membrane, and consequently reducing fouling.

It is worth noting that the decline in flux over time in MD is

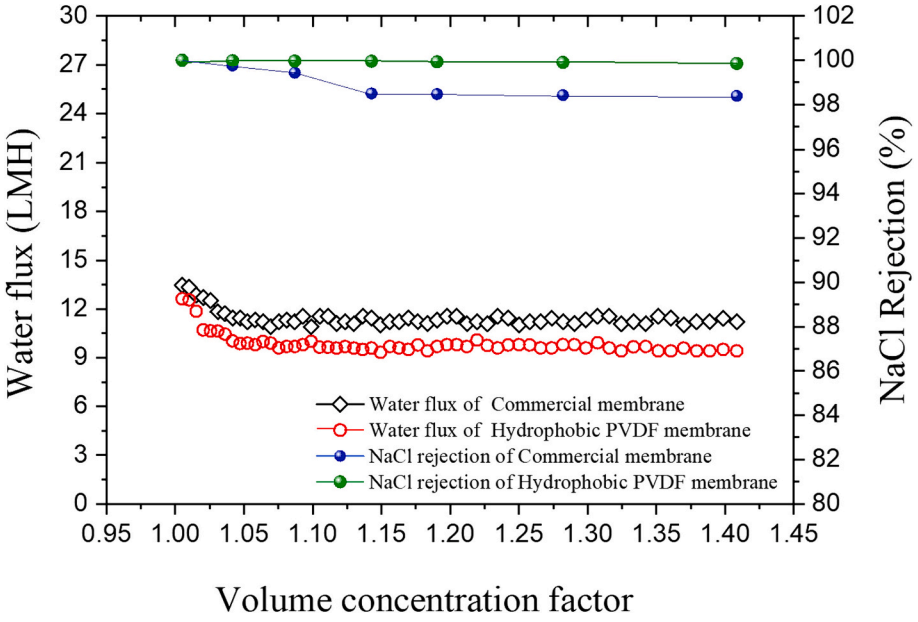

Fig. 4. Performance of the membranes during integrity tests (NaCl concentration = 35 g/L, feed solution temperature = 60 °C, permeate temperature = 20 °C, feed and permeate flow rate = 1.5 LPM).

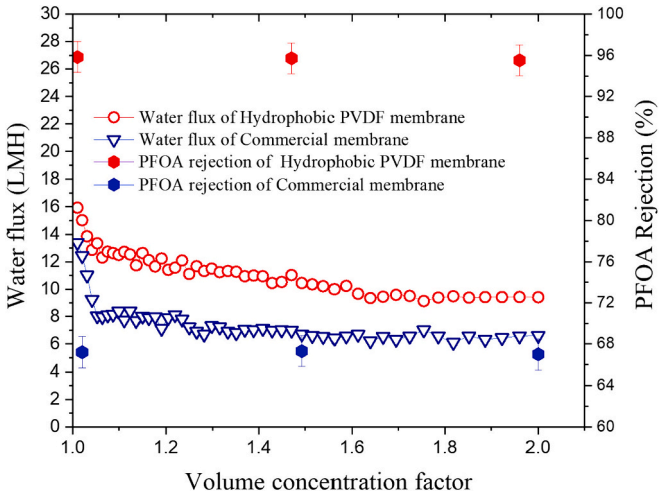

Fig. 5. Water flux and PFOA rejection of PVDF membranes (PFOA concentration = 30 ppm, feed temperature = 60 °C, permeate temperature = 20 °C, flow rate = 1.5 LPM).

influenced by various factors beyond fouling. Understanding these reasons is crucial for optimizing MD processes and maintaining membrane performance. These factors include wetting, decreasing transmembrane temperature as a driving force, and alterations in the feed solution characteristics. While it is evident that PFOA rejection remained constant and flux eventually stabilized during the filtration process, membrane wetting can be dismissed as a concern. However, the gradual reduction in transmembrane temperature and the increase in PFOA concentration within the feed solution over time were inevitable factors that might have contributed, at least partially, to the reduction in flux.

Fig. 5 shows that the fabricated hydrophobic PVDF membrane consistently exhibited a higher permeate flux compared to the commercial membrane. Moreover, the fabricated membrane demonstrated significantly higher rejection (95.8 %) in comparison to the commercial membrane (67.31 %), and this rejection rate remained constant throughout the filtration process. The lower rejection of commercial membranes can be related to the higher tendency of PFOA adsorption to the membrane surface, which can potentially lead to partial pore wetting and a remarkable decrease in PFOA rejection [33].

As depicted in Fig. 6(b), the initial membrane roughness measurements were 43 nm for the commercial PVDF membrane and 76.30 nm for the fabricated hydrophobic PVDF membrane. Following filtration, the roughness of the commercial membrane increased significantly and reached 61.28, while the roughness of the fabricated membrane remained almost unchanged, displaying a value of 78.80 nm. The significant increase in roughness observed in the case of the commercial membrane supports the presence of a more substantial deposition of hydrophobic PFOA foulants on the membrane surface [73].

Fig. 6(c) shows the XPS wide-scan spectra and high resolution of C1s peaks for pristine and fouled fabricated hydrophobic PVDF membranes, illustrating four emission peaks for both membranes at 686.5 eV (F 1s), 530.5 eV (O 1s), 284.5 eV (C 1s), and 101 eV (Si 1s). Fig. 6(d) illustrates the convoluted C1s peaks. Both membranes exhibit two prominent peaks at 286.3 eV (corresponding to $–CH_2–$) and 291.08 eV (representing $–CF_2–$) in their C1s spectra, which indicate the backbone structure of PVDF polymer chains [74,75]. Additionally, the C1s spectra reveal two peaks at 284.9 and 289.25 eV, which can be attributed to the presence of C—H bonds and carbon atoms situated in an electron-withdrawing environment. This environment may arise from functional groups such as ester or amide groups or from bonding with electron-withdrawing atoms such as oxygen (O), indicated by the C═O signature [75]. Analyzing the peak areas of carbon atoms, it is observed that the total carbon atoms percentage of CF_2 and C—H atoms decreases in the used membrane compared to the pristine fabricated hydrophobic PVDF membrane. Conversely, there is an increase in the total carbon atoms percentage of CH_2 and C═O in the C1s spectra of the used membrane. Furthermore, two new peaks emerge at 294.5 eV and 292 eV in the fouled membrane, which can be attributed to $–CF_3–$ and $–CF_2–$ bonds of PFOA [76]. These peaks indicate the attachment of PFOA molecules on the membrane surface, suggesting strong hydrophobic interactions between the PFOA molecules and the membrane surface.

3.3. The effect of operational conditions on the permeate flux in removing PFOA by DCMD

Fig. 7 (a) shows the water flux of the fabricated hydrophobic PVDF

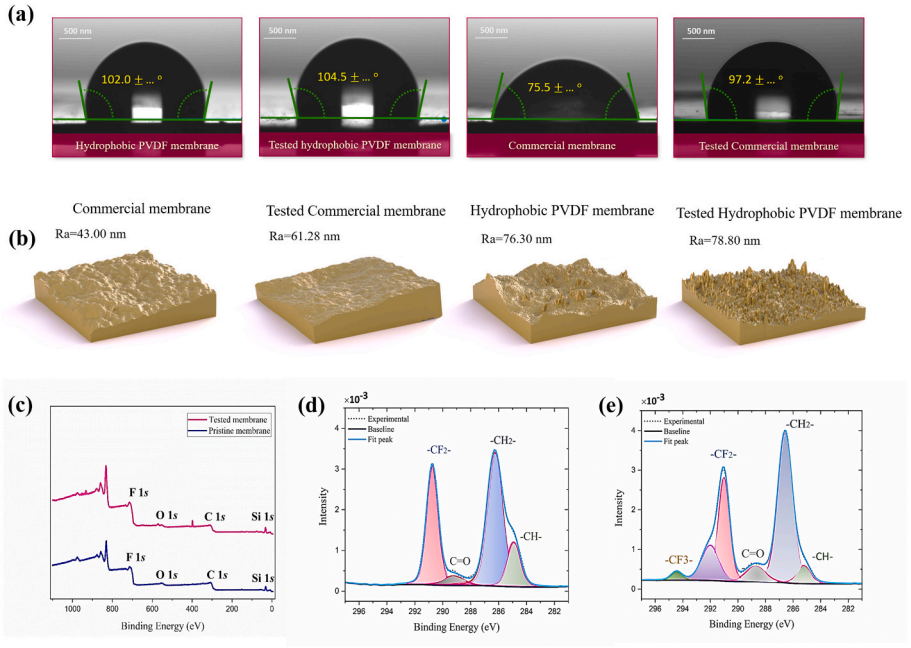

Fig. 6. (a) WCA measurement results for the pristine and tested nanocomposite PVDF membrane, (b) the three-dimensional AFM surface images of the membranes, (c) the XPS survey spectra and deconvoluted C1s peaks of fabricated hydrophobic PVDF membranes, (d) before fouling tests and (e) after fouling tests on PFOA.

membrane with variations in feed temperature, PFOA concentration, and feed flow rate, as determined through an experimental design (detailed information is provided in Supporting Information (Table S1)). The permeate flux is notably influenced by the feed temperature, solute concentration, and crossflow velocity, as these factors tailor the temperature and concentration polarization. The observed trend in flux remained consistent across all runs, showing a significant initial decrease due to fouling, followed by a gradual approach to a steady state over time. The flux continued to decline until a constant effective driving force was established.

Feed temperature was found to be the most significant parameter affecting MD performance. Initial permeate flux (J_0) almost doubled (from 8 to 16 LMH) when feed temperature (T_f) was increased from 40 °C to 60 °C at a constant feed flow rate of 1.5 LPM and PFOA concentration of 30 ppm. However, the impact of the feed flow rate was found to be less significant compared to the feed temperature. When the feed flow rate was increased threefold, from 0.5 to 1.5 LPM, under constant feed temperature (60 °C) and PFOA concentration (10 ppm), the water flux increased from 9 to 15 LMH. The parameter with the least impact is the PFOA concentration. Elevating the PFOA concentration threefold (from 10 to 30 ppm) while maintaining a feed temperature of 60 °C and a feed flow rate of 1.5 LPM, led to only a modest enhancement in water flux, increasing from 16 to 20 LMH.

As the foulant deposition is proportional to the water transport through the membrane, high accumulation typically occurs in the initial operation phases, especially for the high-temperature operation. Therefore, it follows that the higher the initial flux, the greater the decline in flux over time. Furthermore, the PFOA concentration gradient over the membrane surface continuously increases, leading to higher concentration polarization [77]. The best linear fit of the measured water flux between 1 and 1.2 VCF was used to estimate the initial flux decline rates. The upper value (1.2) of this range was identified as the maximum value, and all the curves were linearly fitted with reasonable approximation. Fig. 7(b) shows the initial flux decline as a function of the inlet feed temperature. As expected, a higher flux decline was observed by increasing the feed temperature since the initial flux was higher. The data also allow assessment of the role of the crossflow velocity, in which increasing the crossflow velocity elevated the initial flux decline rate. The higher the feed temperature, the larger the vapor pressure gradient across the membrane, consequently resulting in a higher driving force for water transport. Moreover, elevating crossflow velocity, or larger Reynolds number, resulted in lower heat transfer resistances and lower thickness of the thermal boundary layer, which eventually led to a higher membrane surface temperature and larger water flux. Therefore, raising both the feed temperature and crossflow velocity enhances permeate flux, and higher PFOA concentration on the membrane surface was created, intensifying the concentration polarization effect and increasing the flux decline rate.

Fig. 7(c) indicates the flux decline ratio (FDR = 1- (final water flux/initial water flux)) of the membranes for each experiment. As expected, a higher flux decline was observed by increasing the feed temperature since the initial flux was higher. The results are consistent with Fig. 7(b). It should also be noted that while the water flux at a feed temperature of 60 °C resulted in a higher initial flux (20 LMH), which was approximately twice the flux observed at a temperature of 40 °C (9 LMH), by the end of the tests, it had decreased to 10 LMH, which was only 1.3 times higher than the flux observed at the control condition. Conversely, there was no noticeable flux decline at the lower feed temperature. These findings underscore the rationale for operating at low to medium feed temperatures, specifically at or below 50 °C. Such operational conditions are conducive to mitigating membrane fouling, leading to more consistent and stable performance over time.

The experimental design encompassed 17 DCMD tests, where various combinations of operating parameters, as recommended by the CCD method, were employed to evaluate their significance in MD performance. We investigated PFOA fouling in DCMD under varying feed inlet temperatures, feed flow rates, and feed concentrations. From the results outlined above, we selected two potentially informative response parameters for the response surface analysis: (i) near-stable permeate flux (VCF ranging from 1.6 to 2) and (ii) PFOA rejection. A relative model function was constructed using input data (responses) derived from our experimental findings for these parameters. According to Design Expert, all of these responses exhibited statistical significance concerning feed inlet temperature (T_f), feed flow rate (Q_f), and feed concentration (C_f), as indicated by their low *p*-values and high F-values. The *p*-values obtained from the analysis of variance (ANOVA) and diagnostic plots of PFOA

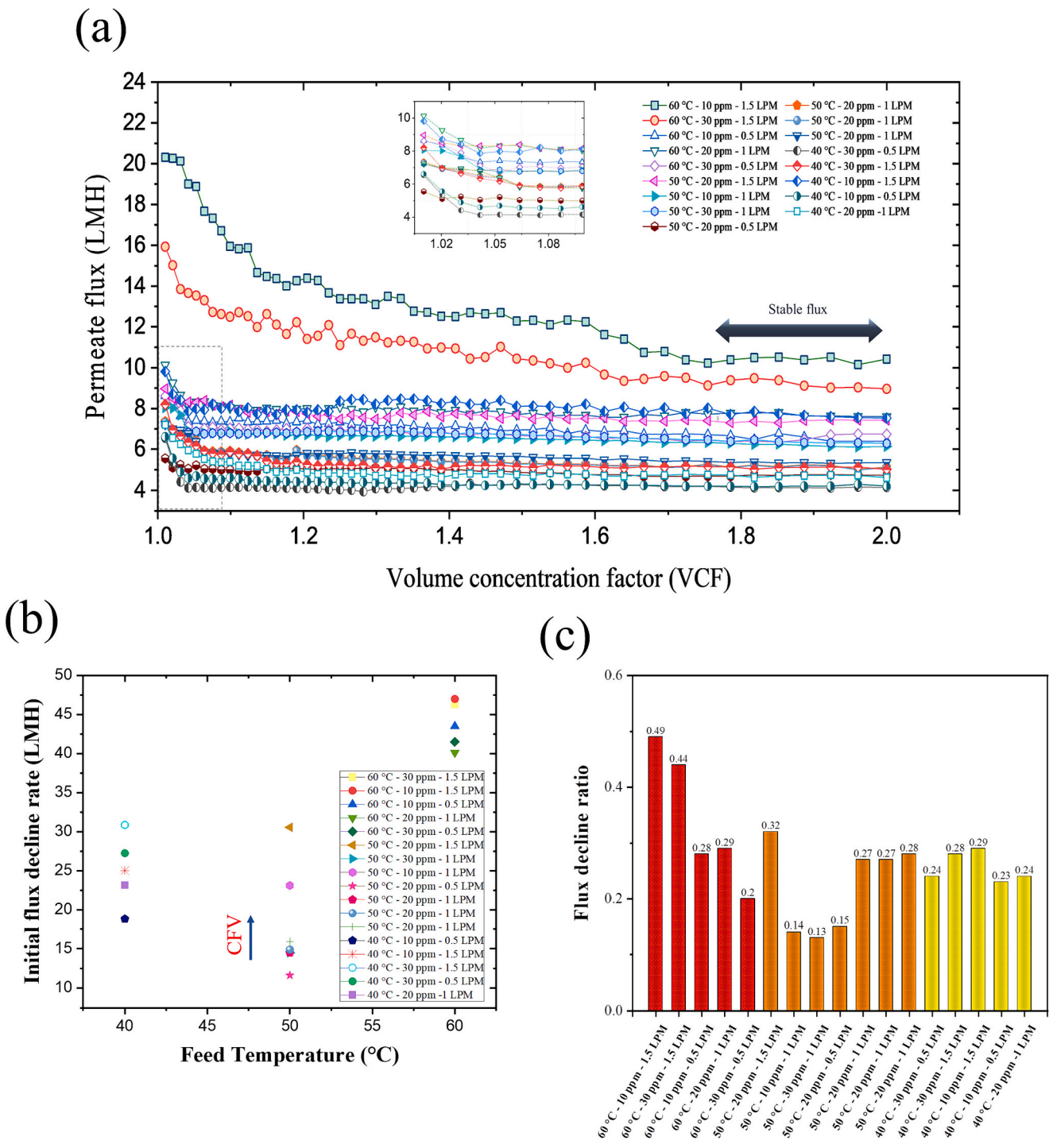

Fig. 7. (a) Results of experiments performed with the synthetic feed water (b) Plot of the initial flux decline rate as a function of the inlet feed temperature (T_f). The arrows indicate the increment of the CFV (c) plot of the flux decline ratio for each experiment.

rejection are summarized in Supporting Information (Table S2, Table S3, and Fig. S2).

Table 3. shows the ANOVA table of the developed model for the permeate flux. The model exhibited a significant F-value of 58.47, with a *p*-value $<10^{-4}$, indicating the adequacy of the reduced quadratic model. Additionally, the R^2-value (coefficient of determination) was impressively high at 0.988, implying that the model accounted for over 98.8 % of the variance in the data. Furthermore, the adjusted and predicted determination coefficients (R^2_{adj} and R^2_{pre}) closely aligned with the R^2, with R^2_{pre} at 0.9385 reasonably consistent with R^2_{adj} at 0.9617. The adequate precision ratio, measuring the signal-to-noise ratio, stood at 27.69, surpassing the desirable threshold of four from a statistical perspective. In light of these findings, it is evident that the developed model is statistically valid for predicting permeate flux within the defined range of factors. Moreover, the significant terms could be ranked based on the F-value or *p*-value; the more significant the *F*-value (smaller *p*-value), the more influential the corresponding coefficient. Thus, in this case, the ranking was as follows: A > B > AB > BC > C > C^2 > A^2. Feed Temperature (*A*) was the most significant factor because it has the highest F value (210.69).

For each response, we present the final equation generated by Design Expert, which establishes the relationship between operating parame-

Table 3
ANOVA analysis for the quadratic model.

Source	Sum of Squares	df	Mean Square	F-value	p-value	
Model	47.76	7	6.82	58.47	< 0.0001	Significant
A-Feed Temperature	24.59	1	24.59	210.69	< 0.0001	
B-Feed flow rate	16.74	1	16.74	143.49	< 0.0001	
C-Feed concentration	0.7398	1	0.7398	6.34	0.0329	
AB	1.34	1	1.34	11.52	0.0079	
BC	1.17	1	1.17	10.03	0.0114	
A^2	0.6092	1	0.6092	5.22	0.0482	
C^2	0.9446	1	0.9446	8.10	0.0192	
Residual	1.05	9	0.1167			
Lack of Fit	1.05	7	0.1496	91.57	0.0108	Significant
Pure Error	0.0033	2	0.0016			
Cor Total	48.81	16				

ters and the respective responses:

$$\text{Permeate flux} = 5.68472 + 1.56800\,T_f + 1.29400\,Q_f + 0.272000\,C_f + 0.410000\,T_fQ_f + 0.382500\,Q_fC_f + 0.448491\,T_f^2 + 0.558491\,C_f^2 \quad (5)$$

These practical models can be readily employed for graphical representation and analysis. Integrating actual data into the predicted model is crucial to ensure its reliability. The model's adequacy was assessed through diagnostic plots, including a normal probability plot of studentized residuals and a plot comparing predicted values to actual values. The diagnostic plots of the permeate rejection and permeate flux are shown in Fig. S2 and Fig. S3, respectively.

Fig. S3(a) shows a plot comparing data to a normal distribution using residuals. A straight line in this plot signifies an even distribution of errors. Fig. S3(b) further illustrates data points clustering around the zero y-axis, indicating consistent variances. Approximately 95 % of the values fall within two standard deviations, reinforcing the assumption of homoscedasticity, which is vital for statistical tests. Fig. S3(c) reveals no discernible trend, indicating that the outcomes are not influenced by the sequence in which the runs were conducted. This lack of a trend supports the reliability of our analysis. Lastly, in Fig. S3(d), the presence of a 45-degree line indicates effective modeling, further corroborating the robustness of our analysis. These diagnostic plots collectively confirm the reliability of our analysis, shedding light on the impact of operational parameters on organic fouling in MD.

Fig. 8 demonstrates the three-dimensional surface response as a function of operating parameters, including feed temperature, feed flow rate, and feed concentration. It also indicates the major effects and the interaction between the investigated parameters. As mentioned earlier, feed temperature notably exerted the most substantial influence on both response variables. Specifically, Fig. 8(a) shows how contour values increase from a permeate flux of 4 to 11 LMH when the T_f increases from 40 to 60 °C. At maximum feed flow rate and concentration, only

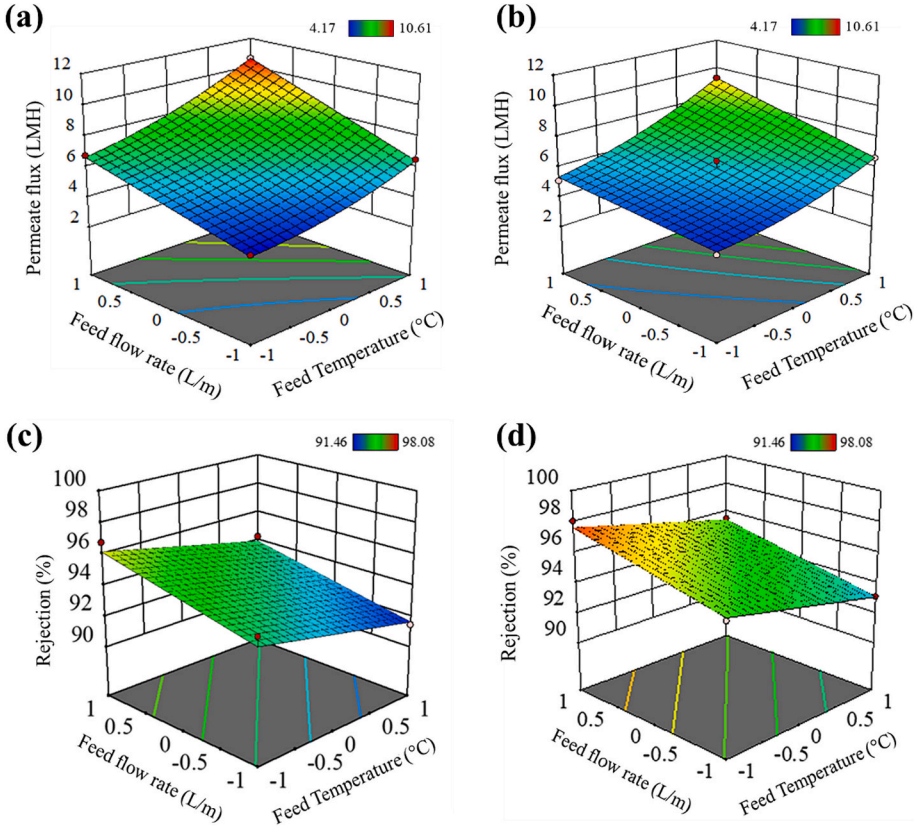

Fig. 8. 3D response surface plot for responses of (a) permeate flux at the high feed concentration, (b) permeate flux at the low feed concentration, (c) rejection at the high feed concentration, and (d) rejection at the low feed concentration.

approximately 1 LMH of stable flux is gained for each 5 °C-step in ΔT_f (Fig. 8(a)). However, a different trend emerges when considering the impact of feed flow rate while varying feed temperature. The permeate flux becomes more sensitive to variations in feed flow rate at higher T_f values (Fig. 8(a)). This observed proportionality can be attributed to the relationship between T_f and temperature polarization. A faster feed flow rate effectively mitigates temperature polarization, and this effect becomes more pronounced when temperature polarization is of greater magnitude, particularly at higher T_f values. This mechanism, in turn, results in a larger J_0 (as seen in Fig. 7) and a steeper decline in flux. Conversely, increasing the feed flow rate yields improved productivity concerning the magnitude of the permeate flux. This enhancement may be attributed to reduced fouling deposition stemming from decreased boundary layer sizes [78,79].

Indeed, the response flux exhibits notable variations across different parameter combinations. The maximum observed response flux reached 11 LMH under specific conditions, characterized by a feed concentration of 30 ppm, a feed temperature of 60 °C, and a feed flow rate of 1.5 L/min. Conversely, the minimum response flux of 4 LMH was recorded under contrasting conditions, featuring a feed concentration of 10 ppm, a feed temperature of 40 °C, and a feed flow rate of 0.5 LPM. In contrast, the behavior of PFOA rejection demonstrates a distinct trend. As illustrated in Fig. 8(c), under conditions of maximum feed concentration (30 ppm) and a flow rate of 0.5 LPM, the rejection rate declined with an increase in feed temperature. Figs. 8(c) and (d) collectively emphasize that the highest rejection rate, approximately 98 %, was achieved under specific conditions, including a feed concentration of 10 ppm, a feed temperature of 40 °C, and a feed flow rate of 1.5 LPM. This outcome underscores a fundamental principle: reduced membrane fouling contributes to higher rejection rates.

4. Conclusions

The present study investigated the potential of DCMD for removing and concentrating PFOA, one of the most widely used PFAS substances, from water using a commercial and fabricated hydrophobic PVDF membrane. Results indicated that substantial fouling occurred on the surface commercial membrane, decreasing PFAS rejection. In comparison, the fabricated PVDF membrane exhibited a significantly improved performance, with an impressive PFOA rejection rate of 98 %. High LEP of fabricated membrane enhances its resilience against wetting. Moreover, the presence of silanol compounds on the surface of the SiO2 nanoparticles contributes to this enhanced negativity. The more negative charge of nanocomposite PVDF membranes enhances their ability to repel negatively charged PFOA molecules through more pronounced electrostatic repulsion. This electrostatic repulsion effectively counteracts the hydrophobic-hydrophobic interaction between PFOA molecules and the membrane surface. This attribute enhances the membranes' resistance to fouling by fluorinated contaminants.

Moreover, RSM was conducted to assess the role of feed temperature, feed concentration, and crossflow velocity in the removal of PFOA by the DCMD process. It was observed that feed inlet temperature exerts a more significant impact on undermining membrane performance than feed flow rate and feed concentration in terms of PFOA rejection and permeate flux. A more severe flux decline was observed at higher feed inlet temperatures, emphasizing the importance of operating at low to medium feed temperatures to achieve feasible fluxes while minimizing the loss of driving force and energy required for heating the feed solution. Indeed, increasing the feed flow rate yields enhanced productivity concerning the magnitude of the permeate flux and PFOA rejection.

CRediT authorship contribution statement

Afrouz Yousefi: Writing – original draft, Methodology, Investigation, Formal analysis, Data curation, Conceptualization. **Kazem Moradi:** Methodology, Investigation, Data curation. **Pooria Karami:** Writing – review & editing, Investigation, Formal analysis, Data curation. **Mostafa Dadashi Firouzjaei:** Writing – review & editing, Investigation, Formal analysis, Data curation. **Mark Elliott:** Writing – review & editing, Project administration, Investigation, Formal analysis. **Ahmad Rahimpour:** Writing – review & editing, Methodology, Investigation, Formal analysis, Conceptualization. **Mohtada Sadrzadeh:** Writing – review & editing, Supervision, Resources, Project administration, Investigation, Funding acquisition, Conceptualization.

Declaration of competing interest

The authors declare that they have no known competing financial interests or personal relationships that could have appeared to influence the work reported in this paper.

Data availability

No data was used for the research described in the article.

Acknowledgments

The financial support for this work by the Natural Science and Engineering Research Council of Canada and Canada's Oil Sands Innovation Alliance (COSIA) is gratefully acknowledged.

Appendix A. Supplementary data

Supplementary data to this article can be found online at https://doi.org/10.1016/j.desal.2024.117509.

References

[1] J. Zhang, H. Pang, S. Gray, S. Ma, Z. Xie, L. Gao, PFAS removal from wastewater by in-situ formed ferric nanoparticles: solid phase loading and removal efficiency, J. Environ. Chem. Eng. 9 (2021) 105452.
[2] S.C.E. Leung, P. Shukla, D. Chen, E. Eftekhari, H. An, F. Zare, N. Ghasemi, D. Zhang, N.-T. Nguyen, Q. Li, Emerging technologies for PFOS/PFOA degradation and removal: a review, Sci. Total Environ. 827 (2022) 153669.
[3] E. Gagliano, M. Sgroi, P.P. Falciglia, F.G.A. Vagliasindi, P. Roccaro, Removal of poly-and perfluoroalkyl substances (PFAS) from water by adsorption: role of PFAS chain length, effect of organic matter and challenges in adsorbent regeneration, Water Res. 171 (2020) 115381.
[4] R. Dhore, G.S. Murthy, Per/polyfluoroalkyl substances production, applications and environmental impacts, Bioresour. Technol. 341 (2021) 125808.
[5] Y. Zhi, H. Lu, K.D. Grieger, G. Munoz, W. Li, X. Wang, Q. He, S. Qian, Bioaccumulation and translocation of 6: 2 fluorotelomer sulfonate, GenX, and perfluoroalkyl acids by urban spontaneous plants, ACS ES&T Eng. 2 (2022) 1169–1178.
[6] M.N. Ehsan, M. Riza, M.N. Pervez, M.M.O. Khyum, Y. Liang, V. Naddeo, Environmental and health impacts of PFAS: sources, distribution and sustainable management in North Carolina (USA), Sci. Total Environ. 878 (2023) 163123.
[7] R. Lohmann, I.T. Cousins, J.C. DeWitt, J. Gluge, G. Goldenman, D. Herzke, A. B. Lindstrom, M.F. Miller, C.A. Ng, S. Patton, Are fluoropolymers really of low concern for human and environmental health and separate from other PFAS? Environ. Sci. Technol. 54 (2020) 12820–12828.
[8] J. Stubleski, S. Salihovic, P.M. Lind, L. Lind, L. Dunder, P. McCleaf, K. Eurén, L. Ahrens, M. Svartengren, B. van Bavel, The effect of drinking water contaminated with perfluoroalkyl substances on a 10-year longitudinal trend of plasma levels in an elderly Uppsala cohort, Environ. Res. 159 (2017) 95–102.
[9] A. Garg, N.P. Shetti, S. Basu, M.N. Nadagouda, T.M. Aminabhavi, Treatment technologies for removal of per-and polyfluoroalkyl substances (PFAS) in biosolids, Chem. Eng. J. 453 (2023) 139964.
[10] I.T. Cousins, J.H. Johansson, M.E. Salter, B. Sha, M. Scheringer, Outside the safe operating space of a new planetary boundary for per-and polyfluoroalkyl substances (PFAS), Environ. Sci. Technol. 56 (2022) 11172–11179.
[11] G.W. Olsen, D.C. Mair, C.C. Lange, L.M. Harrington, T.R. Church, C.L. Goldberg, R. M. Herron, H. Hanna, J.B. Nobiletti, J.A. Rios, Per-and polyfluoroalkyl substances (PFAS) in American Red Cross adult blood donors, 2000–2015, Environ. Res. 157 (2017) 87–95.
[12] T.A. Bruton, A. Blum, Proposal for coordinated health research in PFAS-contaminated communities in the United States, Environ. Health 16 (2017) 120.
[13] H. Lin, Y. Wang, J. Niu, Z. Yue, Q. Huang, Efficient sorption and removal of perfluoroalkyl acids (PFAAs) from aqueous solution by metal hydroxides generated in situ by electrocoagulation, Environ. Sci. Technol. 49 (2015) 10562–10569.
[14] B. Gomez-Ruiz, S. Gómez-Lavín, N. Diban, V. Boiteux, A. Colin, X. Dauchy, A. Urtiaga, Efficient electrochemical degradation of poly-and perfluoroalkyl

substances (PFASs) from the effluents of an industrial wastewater treatment plant, Chem. Eng. J. 322 (2017) 196–204.
[15] J. Niu, Y. Li, E. Shang, Z. Xu, J. Liu, Electrochemical oxidation of perfluorinated compounds in water, Chemosphere 146 (2016) 526–538.
[16] P. Gu, C. Zhang, Z. Sun, H. Zhang, Q. Zhou, S. Lin, J. Rong, M.R. Hoffmann, Enhanced photoreductive degradation of perfluorooctanesulfonate by UV irradiation in the presence of ethylenediaminetetraacetic acid, Chem. Eng. J. 379 (2020) 122338.
[17] M.F. Rahman, S. Peldszus, W.B. Anderson, Behaviour and fate of perfluoroalkyl and polyfluoroalkyl substances (PFASs) in drinking water treatment: a review, Water Res. 50 (2014) 318–340.
[18] S. Rayne, K. Forest, Perfluoroalkyl sulfonic and carboxylic acids: a critical review of physicochemical properties, levels and patterns in waters and wastewaters, and treatment methods, J. Environ. Sci. Health A 44 (2009) 1145–1199.
[19] C. Gallen, D. Drage, G. Eaglesham, S. Grant, M. Bowman, J.F. Mueller, Australia-wide assessment of perfluoroalkyl substances (PFASs) in landfill leachates, J. Hazard. Mater. 331 (2017) 132–141.
[20] Z. Lu, R. Lu, H. Zheng, J. Yan, L. Song, J. Wang, H. Yang, M. Cai, Risk exposure assessment of per-and polyfluoroalkyl substances (PFASs) in drinking water and atmosphere in central eastern China, Environ. Sci. Pollut. Res. 25 (2018) 9311–9320.
[21] M. Greger, T. Landberg, Removal of PFAS from water by aquatic plants, J. Environ. Manag. 351 (2024) 119895.
[22] S. Garg, J. Wang, P. Kumar, V. Mishra, H. Arafat, R.S. Sharma, L.F. Dumée, Remediation of water from per-/poly-fluoroalkyl substances (PFAS)–challenges and perspectives, J. Environ. Chem. Eng. 9 (2021) 105784.
[23] F.S.A. Khan, N.M. Mubarak, M. Khalid, Y.H. Tan, E.C. Abdullah, M.E. Rahman, R. R. Karri, A comprehensive review on micropollutants removal using carbon nanotubes-based adsorbents and membranes, J. Environ. Chem. Eng. 9 (2021) 106647.
[24] K. Moradi, M. Rastgar, P. Karami, A. Yousefi, S. Noamani, A. Hemmati, M. Sadrzadeh, Performance analysis of the Thermo Osmotic Energy Conversion (TOEC) process for harvesting low-grade heat, Chem. Eng. J. Adv. 16 (2023) 100558.
[25] E.W. Tow, M.S. Ersan, S. Kum, T. Lee, T.F. Speth, C. Owen, C. Bellona, M. N. Nadagouda, A.M. Mikelonis, P. Westerhoff, Managing and treating per-and polyfluoroalkyl substances (PFAS) in membrane concentrates, AWWA Water Sci. 3 (2021) e1233.
[26] R.L. Ramos, V.R. Moreira, Y.A.R. Lebron, M.F. Martins, L.V.S. Santos, M.C. S. Amaral, Direct contact membrane distillation for surface water treatment and phenolic compounds retention: from bench to pilot scale, Desalination 574 (2024) 117225.
[27] K.H. Kucharzyk, R. Darlington, M. Benotti, R. Deeb, E. Hawley, Novel treatment technologies for PFAS compounds: a critical review, J. Environ. Manag. 204 (2017) 757–764.
[28] M. Pishnamazi, S. Koushkbaghi, S.S. Hosseini, M. Darabi, A. Yousefi, M. Irani, Metal organic framework nanoparticles loaded-PVDF/chitosan nanofibrous ultrafiltration membranes for the removal of BSA protein and Cr (VI) ions, J. Mol. Liq. 317 (2020) 113934.
[29] A. Kargari, A. Yousefi, Process intensification through magnetic treatment of seawater for production of drinking water by membrane distillation process: a novel approach for commercialization membrane distillation process, Chem. Eng. Process.-Process Intensif. 167 (2021) 108543.
[30] S. Noamani, S. Niroomand, M. Rastgar, M. Azhdarzadeh, M. Sadrzadeh, Modeling of air-gap membrane distillation and comparative study with direct contact membrane distillation, Ind. Eng. Chem. Res. 59 (2020) 21930–21947.
[31] M.M. Damtie, B. Kim, Y.C. Woo, J.-S. Choi, Membrane distillation for industrial wastewater treatment: studying the effects of membrane parameters on the wetting performance, Chemosphere 206 (2018) 793–801.
[32] R.L. Ramos, V.R. Moreira, Y.A.R. Lebron, M.F. Martins, L.V.S. Santos, M.C. S. Amaral, Direct contact membrane distillation for surface water treatment and phenolic compounds retention: from bench to pilot scale, Desalination 574 (2024) 117225.
[33] X. Chen, A. Vanangamudi, J. Wang, J. Jegatheesan, V. Mishra, R. Sharma, S. R. Gray, J. Kujawa, W. Kujawski, F. Wicaksana, Direct contact membrane distillation for effective concentration of perfluoroalkyl substances–impact of surface fouling and material stability, Water Res. 182 (2020) 116010.
[34] A. Deshmukh, C. Boo, V. Karanikola, S. Lin, A.P. Straub, T. Tong, D.M. Warsinger, M. Elimelech, Membrane distillation at the water-energy nexus: limits, opportunities, and challenges, Energy Environ. Sci. 11 (2018) 1177–1196.
[35] H. Cao, Y. Mao, W. Wang, Y. Jin, Y. Gao, M. Zhang, X. Zhao, J. Sun, Z. Song, ZIF-8 based dual scale superhydrophobic membrane for membrane distillation, Desalination 550 (2023) 116373.
[36] C. Li, W. Liu, J. Mao, L. Hu, Y. Yun, B. Li, Superhydrophobic PVDF membrane modified by dopamine self-polymerized nanoparticles for vacuum membrane distillation, Sep. Purif. Technol. 304 (2023) 122182.
[37] Y. Jin, Z. Wei, X. Meng, J. Li, Fabrication of superhydrophobic PVDF membrane via catechol/polyamine co-deposition and SiO2 nanoparticles for membrane distillation, J. Environ. Chem. 11 (3) (2023) 110250.
[38] Z. Lenac, C. Saldías, C.A. Terraza, A. Leiva, J. Koschikowski, D. Winter, A. Tundidor-Camba, R. Martin-Trasanco, Spraying fluorinated silicon oxide nanoparticles on CuONPs@ CF-PVDF membrane: a simple method to achieve superhydrophobic surfaces and high flux in direct contact membrane distillation, Polymers (Basel) 14 (2022) 5164.
[39] J. Lin, J. Du, S. Xie, F. Yu, S. Fang, Z. Yan, X. Lin, D. Zou, M. Xie, W. Ye, Durable superhydrophobic polyvinylidene fluoride membranes via facile spray-coating for effective membrane distillation, Desalination 538 (2022) 115925.
[40] N.A. Zakaria, S.Q. Zaliman, C.P. Leo, A.L. Ahmad, B.S. Ooi, P.E. Poh, 3D imprinted superhydrophobic polyvinylidene fluoride/carbon black membrane for membrane distillation with electrochemical cleaning evaluation, J. Environ. Chem. Eng. 10 (2022) 107346.
[41] S. Lin, S. Nejati, C. Boo, Y. Hu, C.O. Osuji, M. Elimelech, Omniphobic membrane for robust membrane distillation, Environ. Sci. Technol. Lett. 1 (2014) 443–447.
[42] C. Boo, J. Lee, M. Elimelech, Omniphobic polyvinylidene fluoride (PVDF) membrane for desalination of shale gas produced water by membrane distillation, Environ. Sci. Technol. 50 (2016) 12275–12282.
[43] C. Boo, J. Lee, M. Elimelech, Engineering surface energy and nanostructure of microporous films for expanded membrane distillation applications, Environ. Sci. Technol. 50 (2016) 8112–8119.
[44] Z. Anari, A. Sengupta, K. Sardari, S.R. Wickramasinghe, Surface modification of PVDF membranes for treating produced waters by direct contact membrane distillation, Sep. Purif. Technol. 224 (2019) 388–396.
[45] G. Zuo, R. Wang, Novel membrane surface modification to enhance anti-oil fouling property for membrane distillation application, J. Membr. Sci. 447 (2013) 26–35.
[46] Z. Wang, J. Jin, D. Hou, S. Lin, Tailoring surface charge and wetting property for robust oil-fouling mitigation in membrane distillation, J. Membr. Sci. 516 (2016) 113–122.
[47] Z. Wang, D. Hou, S. Lin, Composite membrane with underwater-oleophobic surface for anti-oil-fouling membrane distillation, Environ. Sci. Technol. 50 (2016) 3866–3874.
[48] L. Zhao, C. Wu, X. Lu, D. Ng, Y.B. Truong, Z. Xie, Activated carbon enhanced hydrophobic/hydrophilic dual-layer nanofiber composite membranes for high-performance direct contact membrane distillation, Desalination 446 (2018) 59–69.
[49] J. Zuo, T.-S. Chung, Metal–organic framework-functionalized alumina membranes for vacuum membrane distillation, Water (Basel) 8 (2016) 586.
[50] R. Roshani, F. Ardeshiri, M. Peyravi, M. Jahanshahi, Highly permeable PVDF membrane with PS/ZnO nanocomposite incorporated for distillation process, RSC Adv. 8 (2018) 23499–23515.
[51] J. Zhang, Z. Huang, L. Gao, S. Gray, Z. Xie, Study of MOF incorporated dual layer membrane with enhanced removal of ammonia and per-/poly-fluoroalkyl substances (PFAS) in landfill leachate treatment, Sci. Total Environ. 806 (2022) 151207.
[52] A.L. Ahmad, N.H.M. Yasin, C.J.C. Derek, J.K. Lim, Crossflow microfiltration of microalgae biomass for biofuel production, Desalination 302 (2012) 65–70.
[53] M.J.K. Bashir, H.A. Aziz, M.S. Yusoff, M.N. Adlan, Application of response surface methodology (RSM) for optimization of ammoniacal nitrogen removal from semi-aerobic landfill leachate using ion exchange resin, Desalination 254 (2010) 154–161.
[54] J. Bose, S. Chowdhury, U. Adhikari, J. Sikder, Optimisation of direct contact membrane distillation to enhance brackish water desalination and study polyvinylidene fluoride (PVDF) membrane performance, Comput. Chem. Eng. 181 (2024) 108529.
[55] X. Wu, B. Zhao, L. Wang, Z. Zhang, J. Li, X. He, H. Zhang, X. Zhao, H. Wang, Superhydrophobic PVDF membrane induced by hydrophobic SiO2 nanoparticles and its use for CO2 absorption, Sep. Purif. Technol. 190 (2018) 108–116.
[56] Y.M. Shirke, Y.J. Yu, J.-W. Chung, S.-J. Cho, S.J. Kwon, S.U. Hong, J.-D. Jeon, Hydrophobic hollow fiber composite membranes based on hexadecyl-modified SiO2 nanoparticles for toluene separation, J. Environ. Chem. Eng. 12 (2024) 111819.
[57] M.F. Ismail, B. Khorshidi, M. Sadrzadeh, New insights into the impact of nanoscale surface heterogeneity on the wettability of polymeric membranes, J. Membr. Sci. 590 (2019) 117270.
[58] H.J. Busscher, A.W.J. Van Pelt, P. De Boer, H.P. De Jong, J. Arends, The effect of surface roughening of polymers on measured contact angles of liquids, Colloids Surf. A Physicochem. Eng. Asp. 9 (1984) 319–331.
[59] J.D. Miller, S. Veeramasuneni, J. Drelich, M.R. Yalamanchili, G. Yamauchi, Effect of roughness as determined by atomic force microscopy on the wetting properties of PTFE thin films, Polym. Eng. Sci. 36 (1996) 1849–1855.
[60] M.F. Ismail, M.A. Islam, B. Khorshidi, A. Tehrani-Bagha, M. Sadrzadeh, Surface characterization of thin-film composite membranes using contact angle technique: review of quantification strategies and applications, Adv. Colloid Interf. Sci. 299 (2022) 102524.
[61] L.A.M. Carrascosa, R. Zarzuela, M. Botana-Galvín, F.J. Botana, M.J. Mosquera, Achieving superhydrophobic surfaces with tunable roughness on building materials via nanosecond laser texturing of silane/siloxane coatings, J. Build. Eng. 58 (2022) 104979.
[62] W.A.F.W. AbdulKadir, A.L. Ahmad, O.B. Seng, N.F.C. Lah, Biomimetic hydrophobic membrane: a review of anti-wetting properties as a potential factor in membrane development for membrane distillation (MD), J. Ind. Eng. Chem. 91 (2020) 15–36.
[63] L.-Y. Yu, Z.-L. Xu, H.-M. Shen, H. Yang, Preparation and characterization of PVDF–SiO2 composite hollow fiber UF membrane by sol–gel method, J. Membr. Sci. 337 (2009) 257–265.
[64] K. Valizadeh, A. Heydarinasab, S.S. Hosseini, S. Bazgir, Fabrication of modified PVDF membrane in the presence of PVI polymer and evaluation of its performance in the filtration process, J. Ind. Eng. Chem. 106 (2022) 411–428.
[65] L.M. Jin, S.L. Yu, W.X. Shi, X.S. Yi, N. Sun, Y.L. Ge, C. Ma, Synthesis of a novel composite nanofiltration membrane incorporated SiO2 nanoparticles for oily wastewater desalination, Polymer (Guildf) 53 (2012) 5295–5303.

[66] B.E. Givens, N.D. Diklich, J. Fiegel, V.H. Grassian, Adsorption of bovine serum albumin on silicon dioxide nanoparticles: impact of pH on nanoparticle–protein interactions, Biointerphases 12 (2017).
[67] M.L. Butzen, J.T. Wilkinson, S.R. McGuinness, S. Amezquita, G.F. Peaslee, J. B. Fein, Sorption and desorption behavior of PFOS and PFOA onto a Gram-positive and a Gram-negative bacterial species measured using particle-induced gamma-ray emission (PIGE) spectroscopy, Chem. Geol. 552 (2020) 119778.
[68] M. Sadrzadeh, J. Hajinasiri, S. Bhattacharjee, D. Pernitsky, Nanofiltration of oil sands boiler feed water: effect of pH on water flux and organic and dissolved solid rejection, Sep. Purif. Technol. 141 (2015) 339–353.
[69] M. Hayatbakhsh, M. Sadrzadeh, D. Pernitsky, S. Bhattacharjee, J. Hajinasiri, Treatment of an in situ oil sands produced water by polymeric membranes, Desalin. Water Treat 57 (2016) 14869–14887.
[70] L. Martínez-Díez, M.I. Vazquez-Gonzalez, Temperature and concentration polarization in membrane distillation of aqueous salt solutions, J. Membr. Sci. 156 (1999) 265–273.
[71] S. Noamani, S. Niroomand, M. Rastgar, A. McDonald, M. Sadrzadeh, Development of a self-sustained model to predict the performance of direct contact membrane distillation, Sep. Purif. Technol. 263 (2021) 118407.
[72] M. Elimelech, W.H. Chen, J.J. Waypa, Measuring the zeta (electrokinetic) potential of reverse osmosis membranes by a streaming potential analyzer, Desalination 95 (1994) 269–286.
[73] H. Wu, F. Shen, J. Wang, Y. Wan, Membrane fouling in vacuum membrane distillation for ionic liquid recycling: interaction energy analysis with the XDLVO approach, J. Membr. Sci. 550 (2018) 436–447.
[74] M. Mohammadi Ghaleni, A. Al Balushi, S. Kaviani, E. Tavakoli, M. Bavarian, S. Nejati, Fabrication of Janus membranes for desalination of oil-contaminated saline water, ACS Appl. Mater. Interfaces 10 (2018) 44871–44879.
[75] Y. Zhu, J. Wang, F. Zhang, S. Gao, A. Wang, W. Fang, J. Jin, Zwitterionic nanohydrogel grafted PVDF membranes with comprehensive antifouling property and superior cycle stability for oil-in-water emulsion separation, Adv. Funct. Mater. 28 (2018) 1804121.
[76] L. Liu, Y. Liu, C. Li, R. Ji, X. Tian, Improved sorption of perfluorooctanoic acid on carbon nanotubes hybridized by metal oxide nanoparticles, Environ. Sci. Pollut. Res. 25 (2018) 15507–15517.
[77] F.A. Banat, J. Simandl, Theoretical and experimental study in membrane distillation, Desalination 95 (1994) 39–52.
[78] A. Hausmann, P. Sanciolo, T. Vasiljevic, U. Kulozik, M. Duke, Performance assessment of membrane distillation for skim milk and whey processing, J. Dairy Sci. 97 (2014) 56–71.
[79] Z. Ding, L. Liu, Z. Liu, R. Ma, Fouling resistance in concentrating TCM extract by direct contact membrane distillation, J. Membr. Sci. 362 (2010) 317–325.